3

Derivation of coarse-grain model for shape transformations of mixed surfactant micelles

3.1 INTRODUCTION

Surfactants are amphiphilic molecules which self-assemble in presence of aqueous solvents into a wide variety of macro-aggregates such as spherical micelles, cylindrical micelles, bilayers, vesicles, or nano-discs [Sangwai and Sureshkumar, 2011; Cates and Candau, 1990; Israelachvili *et al.*, 1976]. Micelles are the macro-aggregates where the hydrophilic head-groups are projected outwards to interact with water where the hydrophobic tails form the inner core. Micelles are formed when the surfactant concentration is above the critical micelle concentration [Maibaum *et al.*, 2004] by maintaining a balance between the hydrophobic interactions when the surfactant-water intermix and electrostatic repulsions between the head groups [Tanford, 1974b,a]. The self-assembly of surfactants is a spontaneous phenomenon which gets affected by altering certain physical conditions such as temperature, pressure, concentration and pH. The resemblance between the topological features of surfactant assemblies with biologically important molecules like lipids make them widely applicable in the fields of drug-delivery mechanisms and pharmaceuticals [Kim *et al.*, 2009; Osada *et al.*, 2009]. Additionally, surfactants are quite useful in cosmetic formulations, detergents, soaps, food technology, paints and oil-recovery [Mehrotra *et al.*, 1990; Tadros, 1992; Johannessen and Spildo, 2013].

Different experimental techniques such as dynamic light scattering (DLS), electron microscopy, electron paramagnetic resonance (EPR), nuclear magnetic resonance (NMR), differential scanning calorimetry (DSC), small-angle X-ray scattering (SAXS) have enabled to identify certain micellar properties like shape, size and transition temperatures [Müller-Goymann, 2004; Fourcade *et al.*, 1994; Martini and Ciani, 2009]. In an experimental study conducted on polymeric micelles, sizes of micelles are found to play a fundamental role in biological activities [Yue *et al.*, 2013]. Sizes of micelles can vary from ∼35 nm to ∼145 nm. Smaller micelles accumulate within the kidney; middle-sized micelles which range from 75-115 nm assemble in lungs while the largest ones with size ∼145 nm are accumulated in spleen and liver. Smallest micelles loaded with drug inhibit the tumour growth due to their better permeability. However, micelles with sizes less than 5 nm are inaccessible in experiments.

In recent years, computational studies have also been performed to understand the micellar assembly and the factors which govern the micelle formation. MD simulations are performed on C_nTAB to find the effect of chain length, size and nature of head-groups [Aoun *et al.*, 2015]. The micelle dynamics investigated in this study is found to be independent of chain-length or the form of head-group. Notable mobility of head-groups is attributed to the solvent molecules surrounding them. The middle part of the chains show slowest dynamics, which are responsible for maintaining the spherical organization of the aggregate. The results hence obtained are in good agreement with the experimental findings. Effect of changing the surfactant concentrations and temperature on self-assembly and kinetics of aggregation has been studied for Sodium dodecyl sulphate (SDS) micelles [Sammalkorpi *et al.*, 2007]. A transition in the structure is seen upon changing temperatures. When the temperature is low, the surfactants prefer the formation of crystalline aggregates, whereas at higher temperatures, micellar phase is formed. The model used in this study reproduces the experimental results with high accuracy. Mesoscopic simulation

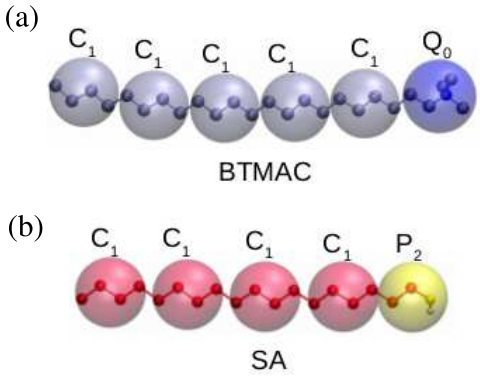

Figure 3.1: Mapping of AA (a) BTMAC and (b) SA to CG degrees of freedom. cpk represents the AA model and the bigger spheres represent the respective CG model. VMD v1.9 [William *et al.*, 1996] is used for the snapshots.

techniques like coarse-graining (CG), have enabled to study the systems of larger size and time scales at a much lower computational cost than the atomistic simulations [Arnarez *et al.*, 2015]. CG simulation of bile salts have shown a tendency to form mixed micelles with different nutrients and with a reduction in stability of the micellar assembly, the nutrients are released inside the intestines [Verde and Frenkel, 2010]. A CG simulation of self-assembly of $C_{12}E_5$ in aqueous solution shows the size of aggregates similar to that with the experiments [Velinova *et al.*, 2011]. Simulations are performed at different concentrations. Upon increasing the concentration, a second critical micelle concentration has been found where the spherical micelles transform to a rod-like shape. The size and the aggregation numbers of the aggregates are well validated with the available experimental results. Additions of drugs in such a system have revealed that about two-thirds of the drug is successfully loaded in the micellar core. The role of hydrogen bonds and electrostatic interactions found to play important roles in stabilizing the micellar phase of 3-hexadecyloxy-2-hydroxy-propyl trimethyl ammonium bromide ($R_{16}HTAB$) [Yan *et al.*, 2019]. The effect of sodium salicilate (NaSaI) is investigated to study the transition in shape for ($R_{16}HTAB$) micelles. The thread like micelles convert into a spherical phase in the absence of NaSaI. The shape remains unchanged in the presence of NaSaI as the aromatic moities of the salicilate ions (SaI^{-1}) align themselves towards the micellar core. SaI^{-1} ions also help in linking two spherical micelles giving a thread-like shape which is favored by hydrogen bonds and electrostatic interactions. Henceforth, from the existing studies it is seen that there are numerous factors which govern the formation and existence of surfactant micelles. Variations in physical parameters such as head-group type, chain length, temperature, effect of ion, concentration, etc. could lead to a significant change in shape and size of the micelle. Hydrogen bonding or electrostatic interactions are also responsible to maintain the stability of the micellar phase. Thus, in order to achieve the desirable shape and size of spherical micelles, a good knowledge of these controlling parameters is necessary.

In the present chapter, all-atom (AA) and coarse-grained (CG) simulations are carried out for two systems: 1) a cationic surfactant and 2) a mixed system of cationic surfactants with co-surfactants. All the simulations are carried out in aqueous medium. Cationic surfactants, behenyltrimethyl ammonium chloride (BTMAC) self-assemble to form cylindrical micelles in water where the shape transforms into a spherical micelles upon adding a co-surfactant, stearyl alcohol, SA. The CG bonded potentials are derived by the Boltzmann inversion of the respective atomistic distributions. MARTINI non-bonded force-field parameters are found to be suitable to obtain the desirable cylindrical micellar phase at the CG level, as obtained at the AA level for the BTMAC/water system. Upon adding the co-surfactant SA, the AA cylindrical micellar phase changes shape to form spherical micelles with a size distribution. The micellar size distribution is not

obtained at the CG level using MARTINI. A systematic parameterization of MARTINI non-bonded parameters enables to obtain the size distributions in the spherical micellar phase consistent with the AA ones. Our simulations show that a correct interplay between the electrostatics, head-group size and hydrophilicity plays an important role in obtaining the micelles of desirable sizes. Thus, this study provides molecular level insights on the controlling parameters of the which play crucial role in cylindrical to spherical shape transformations of the micelles. It also shows the suitability of multi-scale ansatz for exploring the length and time scales relevant to shape transformations which are, otherwise, inaccessible to the experiments.

3.2 COMPUTATIONAL DETAILS

3.2.1 All-atom simulations

The atomistic simulations are carried out for three systems A1 and B1 and B11 (table 3.1) using GROMACSv4.6.5 [Bekker *et al.*, 1993; Abraham *et al.*, 2018; Lindahl *et al.*, 2001; Berendsen *et al.*, 1995; van der Spoel *et al.*, 2005; Hess *et al.*, 2008; Pronk *et al.*, 2013; Páll *et al.*, 2015; Abraham *et al.*, 2015]. The initial configuration of A1 is prepared by randomly placing 100 cationic surfactants, i.e. BTMAC molecules in a cubic box. The box is solvated by 4610 water molecules to maintain a water concentration of 67.83 %. Since BTMAC is a cationic surfactant, 100 chloride ions are also added in the simulation box to maintain the electrical charge balance. The system is energy minimized using the steepest descent algorithm [Leach, 2001]. This is followed by a simulation in an NVT ensemble at 283 K for 100 ps. Next, NPT simulation is carried for 20 ns at 1 bar pressure. The system is coupled to Berendsen thermostat [Berendsen *et al.*, 1984] to achieve the desired temperature with a coupling constant of 0.5 ps. The pressure of the system is maintained at 1 bar using Berendsen barostat [Berendsen *et al.*, 1984]. System B1 is prepared in the similar manner. System size of B11 is kept larger than B1 with same concentration to check the system size effect. Both B1 and B11 are simulated with similar parameters [Lunkad *et al.*, 2017].

Table 3.1: Number of molecules in systems A1, B1 and B11.

Model	System	BTMAC/SA molecules	Water %	NPT (ns)	Final shape of micelle
AA	A1	100/0	67.83	20	Cylindrical
	B1	100/50	84.56	20	Spherical
	B11	400/200	84.56	300	Spherical
CG	A1	100/0	67.83	20	Cylindrical
	B11	400/200	84.56	300	Spherical

3.2.2 Coarse-grained simulations

Mapping scheme

The initial CG configuration is obtained from the final configurations of the respective all atom (AA) simulations of systems A1 and B11. AA BTMAC and SA are mapped into CG representation using VOTCA [Rühle *et al.*, 2009] following the 4:1 mapping scheme of the MARTINI model [Marrink *et al.*, 2007]. The 4:1 mapping is chosen as an optimum to take care of both the computational efficiency of the CG model and the conservation of the chemical nature of the atomistic moiety. To conserve the chemical nature of the underlying atomistic fragment, the CG beads are classified into different types on the basis of polarity. The MARTINI model includes four main bead types: P (polar), N (non-polar), Q (charged) and C apolar. Within each main type, there are subtypes to denote the extent of polarity, denoted by numbers ranging from $1-5$

signifying low-high polarity. The hydrogen bonding capability is distinguished by letters d, a, da or 0 where d = donor, a = acceptor, da = both, 0 = none. These bead types are summarized under table 3.2. Thus, following these notations and definition of the coarse-grained beads, we map atomistic configurations of both BTMAC and SA to obtain their respective CG structures. Figure

Table 3.2: Definition of bead type in the MARTINI model

Type	Notation	Interaction type	Description
Major bead type	P	Polarity	Polar
	N		Non-polar
	Q		Charged
	C		Apolar
Subtype	d	Hydrogen bonding capacity	Donor
	a		Acceptor
	da		Both
	0		None
	1-5	Level of polarity	Increasing from 1 to 5 1: Least, 5: Highest

3.1 shows the mapped structures of BTMAC and SA at CG level and following the mapping scheme presented in table 3.3. The BTMAC and SA head-groups are represented by the bead types Q_0 and P_2 respectively. The tails of both the molecules are represented by bead type of C_1 by combining four atomistic carbons to one bead and Q_a bead type is used to represent the CG chloride ion. The MARTINI CG water is denoted by P_4 bead which is mapped by using four atomistic water molecules. For the effective implementation of orientational polarizability of the real water, the CG water model is parameterized and is referred to as bead type PW. The polarizable water model is a three-bead water model to represent four atomistic water molecules. This modified water model effectively reproduces the dielectric screening of bulk water.

Table 3.3: Mapping scheme for coarse-grained simulation

Molecule	Type	AA	CG bead
BTMAC	Head-group	$C-C-N^+-C_3$	Q_0
	Tail	$C-C-C-C$	C_1
SA	Head-group	$C-C-O-H$	P_2
	Tail	$C-C-C-C$	C_1
Water	Solvent	4 atomistic water	P_4, Standard CG MARTINI water
		Three-bead model, 4 atomistic water	PW, Polarizable CG MARTINI water
Cl	Ion	Cl	Q_a

.

Bonded and non-bonded potentials

Since the bonded CG potentials of BTMAC and SA surfactant molecules are unavailable with the well-established MARTINI force-field, we first derive their bonded CG potentials. To do so, the bonded and the non-bonded potentials are assumed to be independent of each other [Bezkorovaynaya *et al.*, 2012]. The overall potential is written as:

$$U^{CG} = \sum U^{CG}_{bonded} + \sum U^{CG}_{non-bonded} \tag{3.1}$$

The bonded potentials in the above equation are the sum of potentials due to the bonds, angles and dihedrals. Since the analytical functions of the bonded potentials are not known, the CG bonded potentials are derived as tabulated potentials by Boltzmann inversion of the respective atomistic

distributions using [Rühle *et al.*, 2009] the following equation,

$$U(q,T) = -k_B T ln P(q,T), q = r, \theta, \phi \tag{3.2}$$

Similar method of separating variables and similar analytical forms of potentials are used earlier for a diatomic molecule and an aliphatic alkane chain [Poma and Delle Site, 2008]. The poor and unsampled regions obtained from the Boltzmann inversion are smoothened and extrapolated to provide a continuous force. The potentials due to bonds and angles are computed within a minimum-to-maximum range of bonds lengths and bond angles. Bond potentials are computed within a range of 0 nm to box-length which is a distance beyond the non-bonded cut-off distance. Similarly, the angle potentials are computed within a range of 0° to 180°. The non-bonded potentials are taken from the MARTINI force-field where the interactions are calculated by [Marrink *et al.*, 2007],

$$U_{LJ}(r) = 4\epsilon[(\frac{\sigma}{r})^{12} - (\frac{\sigma}{r})^{6}]. \tag{3.3}$$

σ and ϵ are the distance of closest approach and interaction strength between two particles respectively. The electrostatic interactions are computed as:

$$U_{el}(r) = \frac{q_i q_j}{4\pi\epsilon_0\epsilon_r r} \tag{3.4}$$

where q_i and q_j are the charges on i^{th} and j^{th} particle, ϵ_0 is the permittivity of free space. ϵ_r is the relative dielectric constant which is equal to 15 and is meant for explicit screening.

Simulation details

Initial configurations of CG A1 and B11 are obtained from their final atomistic configurations. Simulations are carried out using GROMACSv4.6.5 [Abraham *et al.*, 2018; Bekker *et al.*, 1993; Berendsen *et al.*, 1995; Lindahl *et al.*, 2001; van der Spoel *et al.*, 2005; Hess *et al.*, 2008; Pronk *et al.*, 2013; Páll *et al.*, 2015; Abraham *et al.*, 2015] and VOTCA v1.2.4 [Rühle *et al.*, 2009]. The simulations of both A1 and B11 are carried out using standard CG MARTINI water model However, B11 is also simulated using MARTINI polarizable CG water model to check the influence of water model. Energies are minimized with steepest descent algorithm [Leach, 2001] followed by 100 ps NVT run. The systems are then simulated in an NPT ensemble for 20 ns. The temperature and pressure are coupled at 283 K and 1 bar using velocity re-scale thermostat [Bussi *et al.*, 2007a] and Berendsen [Berendsen *et al.*, 1984] barostat with a coupling constant of 1 ps. The time step for integration is 4 fs and trajectories are collected at every 40 ps. van der Waals and electrostatic interactions are cut-off at 1.2 nm using coulomb type shift.

3.3 RESULTS AND DISCUSSIONS

In A1, the BTMAC molecules self-assemble into cylindrical micelles in both AA and CG simulations. The snapshot of cylindrical micelles obtained from AA and CG simulations of A1 are shown in figures 3.2 (a) and (b) respectively. To check the equilibration of the AA and CG simulations, the solvent accessible surface area (SASA) of BTMAC calculated and its time evolution is monitored. All further analyses for understanding the structural properties of A1 are carried out after the convergence of SASA of BTMAC. To check the suitability of the bonded potentials derived for the CG model, the CG bonded distributions of BTMAC are calculated and compared with respect to their respective AA distributions. Both AA and CG bond distributions for the BTMAC bonds and angles are shown in figure 3.3. The figure shows that the BTMAC bond distribution at CG level match well with the respective atomistic distributions. Thus the potential due to the BTMAC bonds for the CG model are well validated. Similarly, the angle distribution of all the

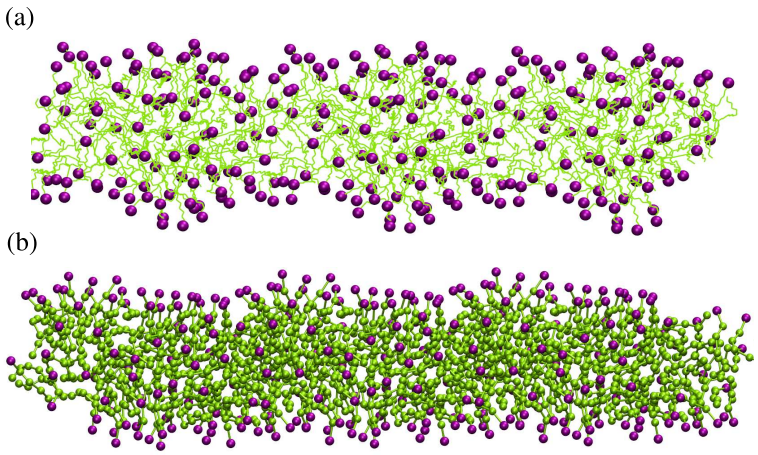

Figure 3.2: Snapshot of BTMAC cylindrical micelle obtained from (a) AA simulation and (b) CG simulation of A1 using MARTINI (M), Water molecules and ions are ignored for the cause of clarity. Color codes: Purple; head, Green; tail

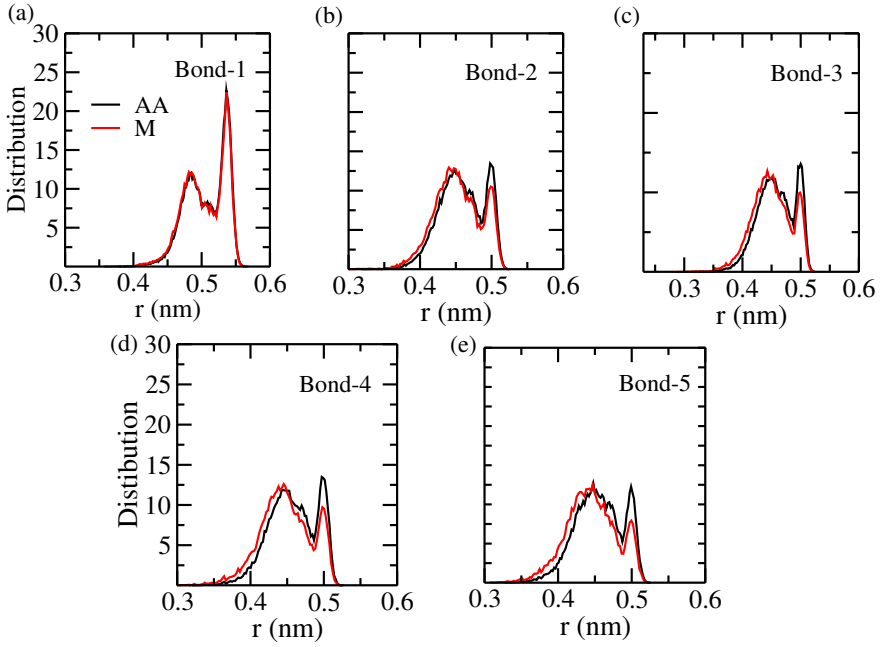

Figure 3.3: Comparison of distribution of BTMAC bonds, AA vs CG in system A1 for (a) bond-1, (b) bond-2, (c) bond-3, (d) bond-4 and (e) bond-5.

angles in BTMAC at both AA and CG levels is shown in figure 3.4. The CG angle distributions however are in reasonable agreement with their respective atomistic distributions. We further compare the non-bonded distributions which majorly govern the self-aggregation phenomena. For this, the radial distribution function, $g(r)$ is computed from equation,

$$g(r) =< \frac{1}{\rho_N} \sum_{i=1}^{N} \sum_{j=1}^{N} \delta(r_{ij} - r) > \tag{3.5}$$

where r_{ij} is the distance between the two particles i, j, N is the total number of particles, ρ signifies mean particle density and the angular brackets denote the time averaging. $g(r)$ determines the local

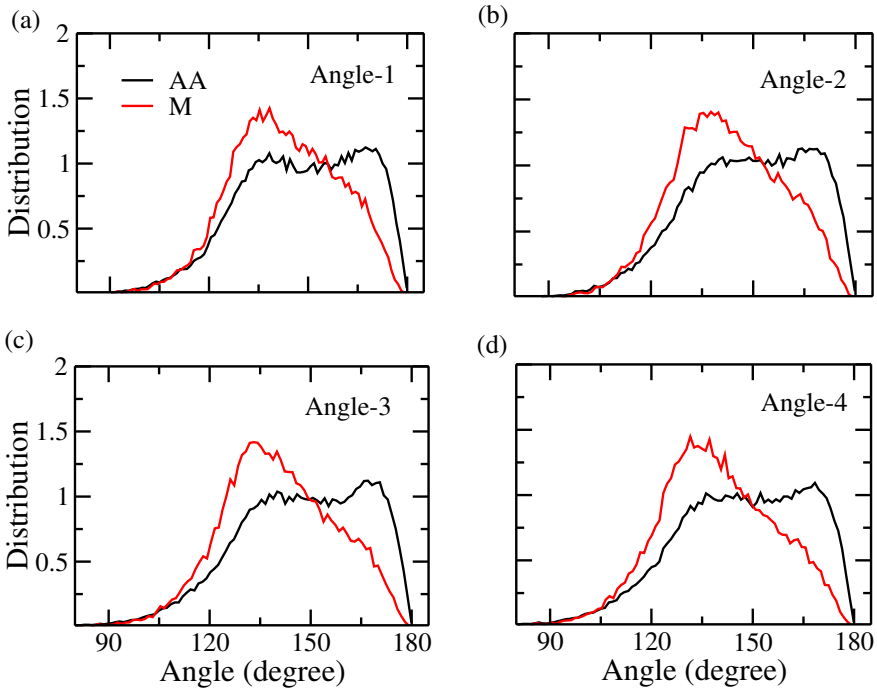

Figure 3.4: Comparison of distribution of BTMAC angles, AA vs CG in system A1 for (a) angle-1, (b) angle-2, (c) angle-3 and (d) angle-4.

arrangement of particles within the aggregate. The center of mass (COM) of the end tail beads is chosen as the reference and $g(r)$ is then computed from the COM of end beads to the surfactant heads. The non-bonded radial distribution function at both AA and CG levels is shown in figure 3.5. The asymmetric nature of $g(r)$ from the centre of mass of end bead to the head, shown in figure 3.5, confirms the presence of cylindrical micelles of the same size in both levels of resolutions. This shows that although the CG angle distributions of BTMAC are in reasonable agreement with their corresponding AA distributions, the derived bonded potentials and the non-bonded force-field parameters from MARTINI are suitable to obtain the desirable micellar phase. Hence the MARTINI model is found to be well-suited to obtain the desired cylindrical symmetry for a surfactant-water system.

Table 3.4: Non-bonded parameters used in CG B11 where M, M_a and M_b represent the MARTINI model and their modifications respectively. PM is the polarizable MARTINI water model.

Molecule	Parameter	M	PM	M_a	M_b
BTMAC	σ, Q_0 (nm)	0.47	0.47	0.52	0.52
	ϵ, Q_0 $(kJmol^{-1})$	3.5	3.5	3.6	3.5
SA	σ, P_2 (nm)	0.47	0.47	0.32	0.32
	ϵ, P_2 $(kJmol^{-1})$	4.5	4.5	7.7	6.6

For system B11, it has been found earlier that BTMAC and SA molecules at a ratio of 2:1 with water concentration of 84.56% wt. self-assemble to give spherical micelles [Lunkad *et al.*, 2017]. The atomistic simulation show that B11 forms 10 spherical micellar aggregates which are classified into three categories, $M1$, $M2$ and $M3$. These three categories differ in terms of radius of the micelle which are ∼2.5 nm, ∼2 nm and ∼1.6 nm for $M1$, $M2$ and $M3$ respectively. Next, a CG model is derived for B11 following similar protocol as in A1 with MARTINI non-bonded potentials referred to as M in table 3.4 using the standard CG water model. The non-bonded

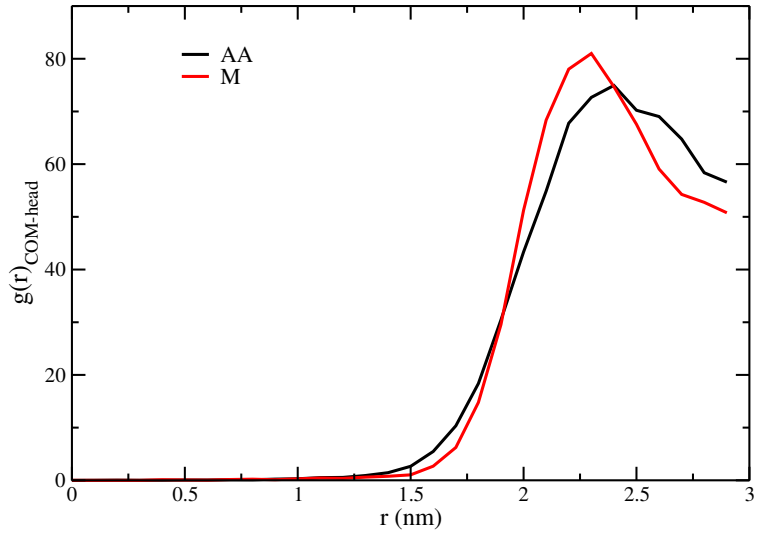

Figure 3.5: g(r) of BTMAC head with respect to the centre of mass of all tails. The AA and CG g(r) match well with each other confirming the shape of the micelle to be cylindrical.

parameters, σ and ϵ for BTMAC head group (denoted by Q_0) and SA head group (denoted by P_2) using the MARTINI force-field (M) are given in the table 3.4 respectively. Since MARTINI does not capture the size distribution of AA micelles, modifications in non-bonded parameters (σ, ϵ) of M are necessary. The modified force-fields are referred to as PM, M_a and M_b in table 3.4. PM utilizes the CG polarizable MARTINI water model, whereas M_a and M_b are obtained after modifications in σ or ϵ in M in presence of standard CG water model. The cross-interactions due to the modified non-bonded terms are computed according to the following equations,

$$\sigma_{ij} = \frac{1}{2}(\sigma_{ii} + \sigma_{jj}) \tag{3.6}$$

$$\epsilon_{ij} = (\epsilon_{ii}\epsilon_{jj})^{\frac{1}{2}} \tag{3.7}$$

where i and j represent the i^{th} and the j^{th} particle respectively. The force-field parameters of all the models are summarized under table 3.4 and are explained in further discussions.

To check the suitability of bonded potentials for CG B11 system, the CG bonded distributions of BTMAC and SA are plotted and compared with their respective atomistic distributions. Figure 3.6 (a) and (b) show the distributions of bond-1 for both BTMAC and SA. From the figure, it is seen that the bond distributions match very well with the AA ones for all models mentioned in the table 3.4. Similarly, the angle distributions of angle-1 for both BTMAC and SA are shown in figure 3.6 (c) and (d). Bonded distributions from all models match reasonably well to the respective AA distributions. The bonded distributions due to other bonds and angles of both the molecules also match reasonably well and are not shown here.

Next, the size distribution of the micellar aggregates using the MARTINI model (M) is shown in figure 3.7 (red color). The AA model forms three classes of micelles, where M leads to the formation of a single aggregate with a higher radius. This can be a probable outcome of mismatched hydrophilic interaction of surfactant heads and the water beads. To understand the role of hydrophilicity and electrostatics arising due to water and head-group interactions, the polarizable MARTINI water model is used in the simulation. This force-field is referred to as PM and the force-field parameters are mentioned in table 3.4. It is seen from figure 3.7 that the PM model does not control the shape and size of the aggregate. The surfactants again self-assemble to form the a spherical micellar aggregate with similar size distribution as obtained from M. This indicates

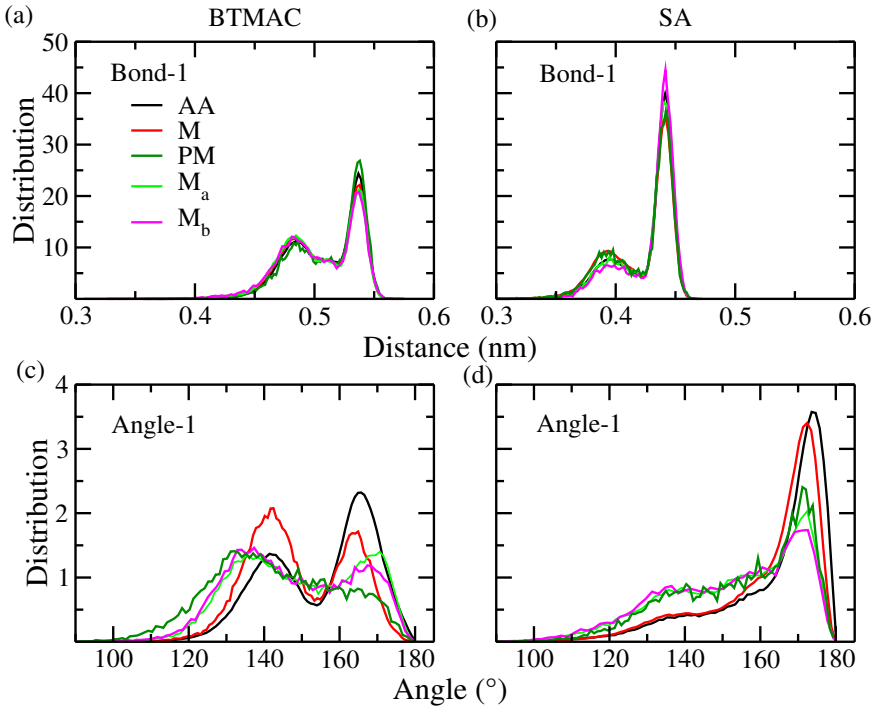

Figure 3.6: AA vs CG bonded distributions in system B11 for bonds in (a) BTMAC, (b) SA and for angle distributions in (c) BTMAC and (d) SA. CG BTMAC and SA bonded distributions match well with the AA ones for all models. CG angle distributions match reasonably well with the AA ones.

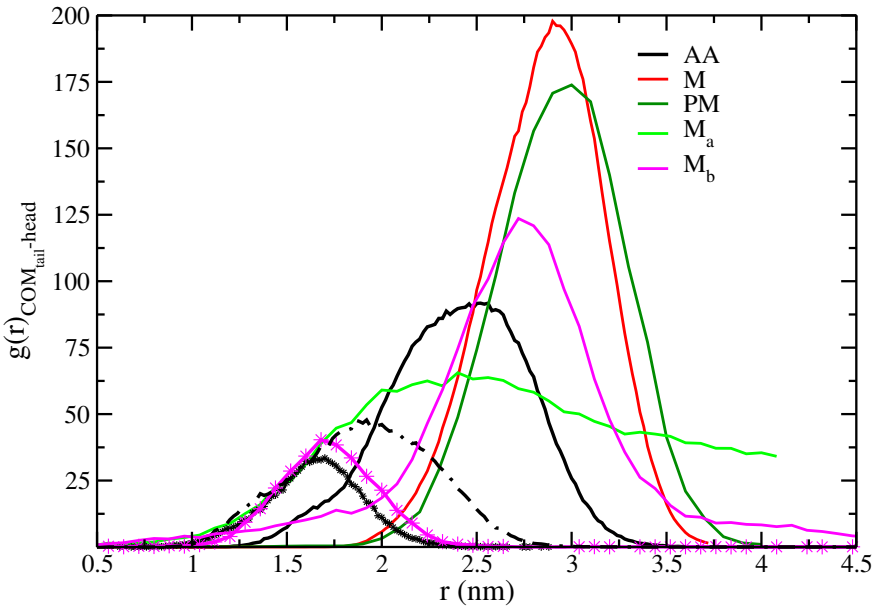

Figure 3.7: g(r) of head beads from the centre of mass of end bead for B11, showing the micellar size distributions from all CG models. Model M_b results in the best match in to the AA ones.

that the water model is not the controlling parameter in the aggregation and size-distribution of

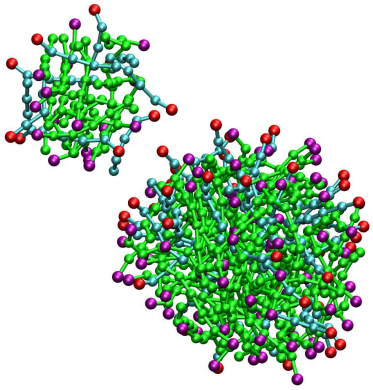

Figure 3.8: Snapshot of self-assembled spherical micelle formed from CG simulation in system B11 using M_b. Color codes: Purple; BTMAC head, Green; BTMAC tail, Red; SA head, Cyan; SA tail.

spherical micelles.

Since MARTINI or polarizable MARTINI models do not reproduce the size distributions of the AA spherical micelles, σ, ϵ of BTMAC and SA heads are re-parameterized based on their excluded volume in the AA force-field. The parameterization scheme is listed in table 3.4. Size of Q_0 and interactions by P_2 are increased from M to M_a. Hence a higher attractive potential among the molecules shrinks the size and results into a single aggregate in M_a. Also, M_a does not lead to the formation of spherical micelles but forms cylindrical aggregate, as seen from the shape of $g(r)$ using this force-field (shown in green color). This indicates that further modifications in the present model are necessary to obtain the spherical micelles with desirable size distributions. Hence another model M_b is developed with the non-bonded parameters listed in table 3.4.

In the model M_b, σ and ϵ of BTMAC heads with bead type Q_0 are kept same as in M. To avoid fusion of aggregates, we reduce the ϵ value of SA head P_2 from M_a which decreases the interactions of SA heads. This results in obtaining a size distribution similar to the AA ones where spherical micelles of two distinct radii of $\sim$1.5 nm and $\sim$2.7 nm are formed as seen in figure 3.7 (magenta color). The symmetry of $g(r)$ clearly demonstrates the formation of spherical micelles. Thus, a correct interplay between hydrophilicity measured in terms of interaction strengths of SA and packing parameter controlled by the sizes of head group leads to obtain the size distributions at the CG level similar to the AA spherical micelles. Figure 3.8 shows the snapshot of the self-assembled spherical micelle of two sizes from model M_b.

3.4 SUMMARY AND CONCLUSIONS

Surfactant BTMAC, in water, self assemble into cylindrical micelles (A1) which transforms to spherical micelles (B11) upon addition of co-surfactant SA from both all-atom and coarse-grained simulations. The bonded potentials for the respective CG models are derived from the Boltzmann inversion of the respective AA simulations and the non-bonded potentials are obtained from MARTINI. The bonded distributions of CG models of BTMAC and SA match reasonably well with their respective atomistic distributions for both A1 and B11 systems. This validates the suitability of the derived bonded potentials for the CG models. Although MARTINI is found to capture the cylindrical micellar phase of the AA A1 system, it does not reproduce the size distributions of spherical micelles for the mixed surfactant/water system, B11. The polarizable CG water model from standard MARTINI to polarizable MARTINI does not influence the aggregation behavior.

This indicates that the water model is not the controlling parameter for the obtaining desirable size of aggregates. Hence the MARTINI force-field is modified by tuning the non-bonded parameters of the model. The head group sizes of BTMAC and SA and interactions strength of SA heads are found to play major roles in the packing and hydrophilicity of the surfactants in water.

Our analyses reveal that an intricate balance between the packing and hydrophilicity results in controlling the size distributions of the CG spherical micelles as in the AA one. The transformation of micelles from the cylindrical to the spherical shape due to the addition of co-surfactants to the surfactants is achieved by re-parameterizing non-bonded potentials of MARTINI guided by packing parameter and hydrophilicity. The current study provides insights on the applicability of dual-scale ansatz for a mixed surfactant system and lays a foundation to derive a generic model for phase transformations at the relevant time and length scale. This will be useful to tune the micellar phase relevant to desired functionalities with industrial and pharmaceutical applications.

Publication: **Arpita Srivastava** and Ananya Debnath, Cylindrical to Spherical Shape transformations of Micelles using All-Atom and Coarse-Grained Molecular Dynamics Simulations **2019**, AIP Conference Proceedings, *2142*, 130004.